JPE 11-6-18

Radial Basis Function Neural Networks (RBFNN) and p-q Power Theory Based Harmonic Identification in Converter Waveforms

Eyad K. Almaita† and Johnson A. Asumadu*

†* Dept. of Electrical and Computer Eng., Western Michigan University, Michigan, USA

Abstract

In this paper, two radial basis function neural networks (RBFNNs) are used to dynamically identify harmonics content in converter waveforms based on the p-q (real power-imaginary power) theory. The converter waveforms are analyzed and the types of harmonic content are identified over a wide operating range. Constant power and sinusoidal current compensation strategies are investigated in this paper. The RBFNN filtering training algorithm is based on a systematic and computationally efficient training method called the hybrid learning method. In this new methodology, the RBFNN is combined with the p-q theory to extract the harmonics content in converter waveforms. The small size and the robustness of the resulting network models reflect the effectiveness of the algorithm. The analysis is verified using MATLAB simulations.

Key Words: Harmonics, Neural networks, P-q theory, Power quality, Radial basis function

I. INTRODUCTION

With the proliferation of nonlinear loads in power systems, harmonic pollution has become a serious problem that affects the power quality in both transmission and distribution systems. The problems caused by harmonics include the malfunctioning of fuses or circuit breakers relays, the heating of conductors and motors, insulation degradation, and communication interference [1]–[3].

Passive filters have been used to compensate for harmonic voltages and currents. Even though passive filters are cheap and easy to operate, they have a low harmonic bandwidth, can be subjected to resonance, have a large size, and are affected by source impedance [4]. However, active power filters (APF), which are more dynamic, have been introduced as an effective means to overcome the problems associated with passive filters. An APF measures the distorted signal and based on a harmonic detection algorithm, decomposes the distorted signal into its fundamental component and other harmonic components. The active filter then uses a power electronics based circuit to

compensate for the harmonic components, the reactive power, and any other distortion (such as unbalanced waveforms). Harmonic detection techniques have been extensively studied. They can be categorized into three main techniques; (i) time domain filters, (ii) frequency domain filters, and (iii) artificially intelligent techniques [5]–[8]. With time domain filters there is a tradeoff between the attenuation and the phase delay (the higher the attenuation the higher the phase delay and vice versa), and a faster transition time can result in oscillations [7]. The main problem with frequency domain filters is that they are not real-time filters [7]. Artificially intelligent filters have been introduced to overcome the disadvantages of time and frequency domain filters. The three main techniques used in artificially intelligent filtering are (i) adaptive linear neuron (ADALINE), (ii) the popular back propagation neural networks (BPNN), and (iii) radial basis neural networks (RBFNN). The ADALINE is used as an online harmonics identifier and its performance depends on the number of harmonics included in its structure. The convergence of the ADALINE slows as the number of harmonics included increases and it is also subject to falling into a local minima [9], [10]. The BPNN on the other hand, deals with the harmonic detection problem as a pattern recognition problem. It uses offline supervised training to identify selected harmonics. However, the long training time required in the BPNN and the chance of falling into local minima are always present [11], [12]. The RBFNN has several advantages over the ADALINE and the BPNN. It is capable of approximating highly nonlinear functions, its structural nature facilitates the training process, because the training can be done in a sequential manner, and the use of local approximation can give better generalization capabilities [11], [12]. Although the RBFNN has been used for harmonic detection, the number of hidden neurons is still large and it still uses an algorithm similar to that of the BPNN. This makes RBFNN networks subject to the same problem found

Manuscript received Nov. 5, 2010; revised Sep. 10, 2011
Recommended for publication by Associate Editor Kyo-Beum Lee.
† Corresponding Author: eyad.k.almaita@wmich.edu
Tel: +1269-7790830, Fax: +1269-276-3151, Western Michigan University
* Dept. of Electrical and Computer Eng., Western Michigan University, USA

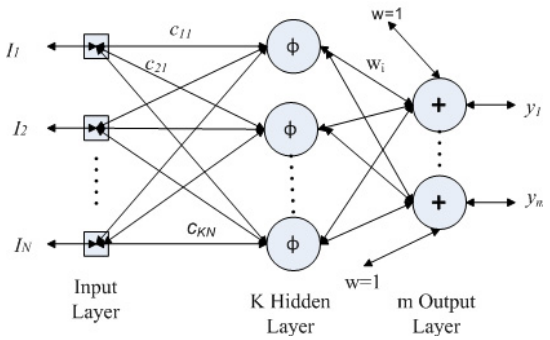

Fig. 1. Structure of RBFNN Network.

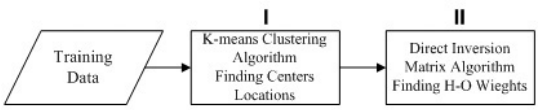

Fig. 2. Block Diagram for the RBFNN Hybrid Learning Process.

in the BPN [9].

In this paper, the RBFNN has been used to identify the total harmonic content in power electronics converter waveforms based on the p-q theory [13]. The novelty of this method is the use of the RBFNN training technique based on a separate and sequential method called the hybrid leaning process. In this method, the centers of the RBFNN were selected based on the K-means clustering method. The weights of the networks are found based on the direct inversion method. In the p-q theory, the total real power (p) contains the constant real component ($\bar{p}$)due to the fundamental components of the voltage and the current plus the oscillating part ($\tilde{p}$)due to all of the other harmonics. In a similar fashion, the reactive power (q) has two similar components; $\bar{q}$ and $\tilde{q}$. In this paper, the oscillating power components $\tilde{p}$ and $\tilde{q}$ are extracted using the RBFNN. Decomposing the active and reactive powers into their components enables a high flexibility in the compensation strategies, as will be shown later in this paper. The results show that the algorithm used for the RBFNN is very effective in terms of the size of the network and requires a short training time.

II. RBFNN Algorithm

A. Structure of the RBFNN

The RBFNN structure consists of three different main layers, as shown in Fig. 1. One is an input layer (source nodes with the inputs I_1, I_2,.., I_N), one is a hidden layer (has K neurons), and one is an output layer (with the outputs y_1, y_2,.., y_m). The input-output mapping consists of two different transformations; a nonlinear transformation from the input layer to the hidden layer and a linear transformation from the hidden to the output layer. The connections between the input layer and the hidden layer are called centers and the connections between the hidden layer and output layer are called weights [11], [12].

The most common radial basis function used in the RBFNN is given by:

$$\phi_i(x) = \exp\left[-\frac{(x-c_i)^T(x-c_i)}{2\sigma_i^2}\right], \quad i = 1,2,\ldots,K. \qquad (1)$$

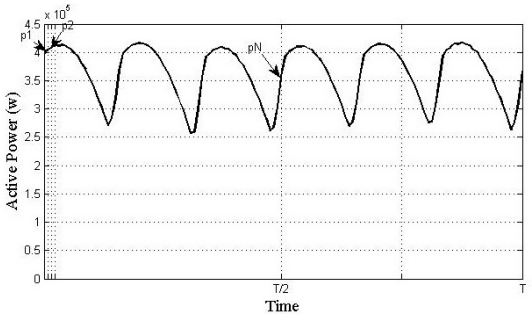

Fig. 3. Steady-State Active Power Waveform.

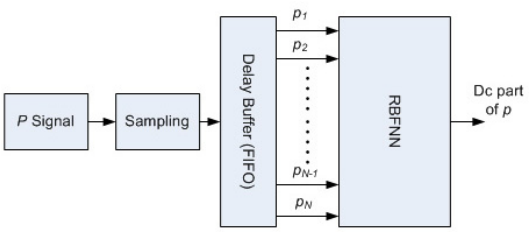

Fig. 4. The Block Diagram for the Input and Output signals for the RBFNNN model.

This is a Gaussian basis function, where φ_i is the output of the i^{th} hidden neuron, x is the input vector data sample (I_1, I_2,…,I_N) (could be the training, the actual, or the test data), c_i is the centers vector of the i^{th} hidden neuron (c_{i1}, c_{i2},..., c_{iN}), σ_i is the normalization factor, and $(x\text{-}c_i)^T(x\text{-}c_i)$ is the square of the vector $(x\text{-}c_i)$ [11] – [12]. The i^{th} output node y_i is a linear weighted summation of the outputs of the hidden layer and is given by:

$$y_i = w_i^T \phi(x), \quad i = 1,2,\ldots,m \qquad (2)$$

where w_i is the weight vector of the output node and $\phi(x)$ is the vector of the outputs from the hidden layer (augmented with an additional bias which assumes a value of 1).

B. Training Algorithm of the RBFNN

The block diagram shown in Fig. 2 illustrates one of the RBFNN training processes called the *hybrid learning* process [14]. The *hybrid learning* process has two different stages; (i) finding suitable locations for the radial basis functions centers of the hidden neurons [12], [14] and (ii) finding the weights between the hidden layer and output layer. In the first stage, the K-means [12], [14] clustering algorithm is used to locate the centers in the input data space regions, where significant data are present (shown as I in Fig. 2). In the second stage (shown as II in Fig. 2) the weights between the hidden layer and the output layer are found by the linear matrix inversion algorithm based on the least-square solution, which minimizes the sum-squared error function [15].

The weights matrix w is given by:

$$w = A^{-1}\Phi^T D \qquad (3)$$

where D is the desired output vector for l training data sample

sets and is given by:

$$D = \begin{bmatrix} d(x_1) \\ \vdots \\ d(x_j) \\ \vdots \\ d(x_l) \end{bmatrix} \quad (4)$$

where $d(x_j)$ describes the output vector corresponding to the j^{th} training data samples vector (x_j). Φ is a matrix where each element $\varphi_i(x_j)$, is a scalar value and represents the output of the i^{th} hidden neuron for the j^{th} training data samples vector (x_j). The Φ matrix for l training data samples is given by:

$$\Phi = \begin{bmatrix} \phi_1(x_1) & \phi_2(x_1) & .... & \phi_K(x_1) \\ \phi_1(x_2) & \phi_2(x_2) & ... & \phi_K(x_2) \\ . & . & & . \\ . & . & ... & . \\ \phi_1(x_l) & \phi_2(x_l) & ... & \phi_K(x_l) \end{bmatrix}. \quad (5)$$

A^{-1} is the variance matrix and is given by:

$$A^{-1} = \left[\Phi^T \Phi\right]^{-1}. \quad (6)$$

One of the advantages of this method when compared to other training algorithms is that it does not need iterations in the training phase. What it needs is the matrix inversion shown in (6), which requires a negligible time to be calculated.

III. Methodology

A. p-q theory

A summary of the p-q theory and an example are shown in Appendix I.

B. RBFNN Method

1) Building the Delay Buffer: Figure 3 shows an example of an instantaneous active power waveform.

Data is sampled at a constant rate and *is passed through a first-input-first-output (FIFO) buffer to create a delayed vector a with length of N, which match the length of the input vector of the R*BFNN. At any instant the FIFO buffer will contain N data samples. As an illustration for the building of the FIFO buffer, the first training data sample x_1 is given by:

$$x_1 = \begin{bmatrix} p_{11} = p_1 \\ p_{21} = 0 \\ \vdots \\ p_{N1} = 0 \end{bmatrix}. \quad (7)$$

The second training data sample x_2 is given by:

$$x_2 = \begin{bmatrix} p_{12} = p_2 \\ p_{22} = p_1 \\ \vdots \\ p_{N2} = 0 \end{bmatrix}. \quad (8)$$

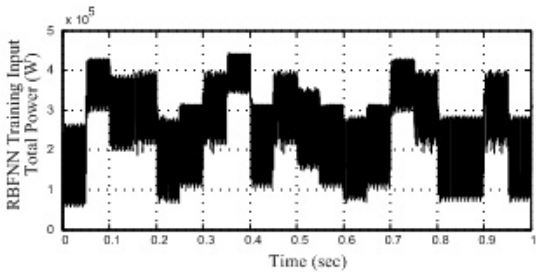

(a)

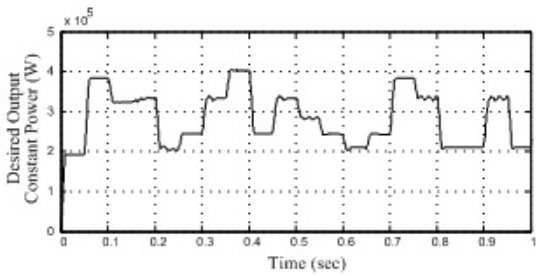

(b)

Fig. 5. Window of Training Data for the Active Power RBFNN Network.

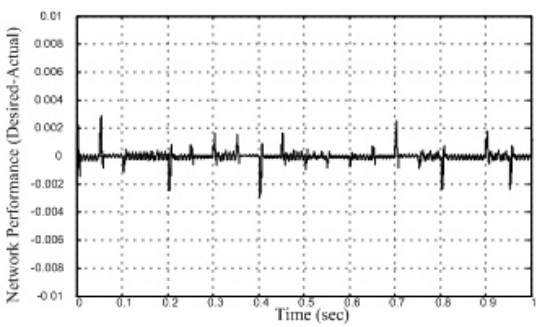

Fig. 6. p- RBFNN Network Performance for Recalling Process

The j^{th} training data sample is given by:

$$x_j = \begin{bmatrix} p_{1j} = p_j \\ p_{1j} = p_{j-1} \\ \vdots \\ p_{N2} = p_{j-N-1} \end{bmatrix}. \quad (9)$$

The training data for l training data samples is written in matrix form and given by:

$$X = \begin{bmatrix} x_1 & x_2 & \cdots & x_l \end{bmatrix} = \begin{bmatrix} p_{11} & p_{12} & \cdots & p_{1l} \\ p_{21} & p_{22} & \cdots & p_{2l} \\ \vdots & \vdots & \cdots & \vdots \\ p_{N1} & p_{N2} & \cdots & p_{Nl} \end{bmatrix}. \quad (10)$$

2) Finding the Desired Output: For each x_j the fast Fourier transform (FFT) is used to find the constant (DC) part of the active power (which represents the power due to the fundamental components). The constant part obtained from applying the FFT on x's data becomes the desired output mentioned in (4).

$$FFT\{x_j\} = d_j{}^{DC}. \quad (11)$$

Note that only the DC component of the FFT is taken, which is a scalar quantity, not a vector as generalized by (4), since

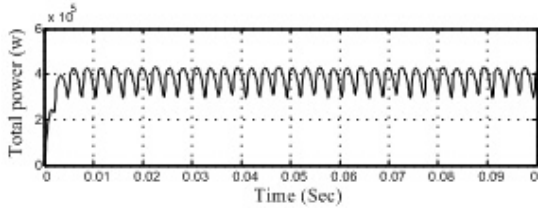

(a)

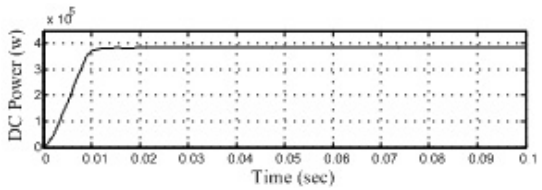

(b)

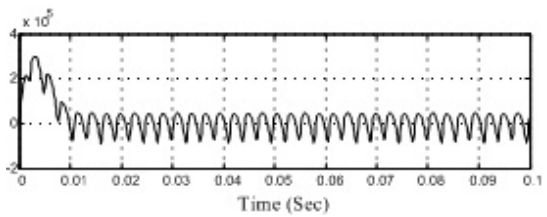

(c)

Fig. 7. Active Power Consumed by the Three-Phase Rectifier. (a) Total. (b) DC Part. (c) Oscillating Part.

the number of output nodes is one. The desired output vector obtained from applying the FFT on each x_j is given by:

$$D = \begin{bmatrix} d_1{}^{DC} \\ \vdots \\ d_j{}^{DC} \\ \vdots \\ d_l{}^{DC} \end{bmatrix}. \tag{12}$$

The training data samples from matrix X of (10) is the same data used by the K-means clustering algorithm to find the centers vectors (c_1, c_2,..., c_K) used in (1). The Gaussian radial basis function of (1) is then used to find the matrix ϕ of the hidden neurons outputs. The weights vector w can then be found using (3).

In a similar fashion the steps used in section III (A1 and A2) to train the network, to extract the DC part of the active power, are repeated for the imaginary power.

3) Embedding the RBFNN Model in the System: After obtaining the RBFNN models parameters (centers and weights) for both the active and imaginary powers, from the training process, the RBFNN model is now ready to be tested. Fig. 4 shows a block diagram for the input and output signals of the RBFNN model for the active power network. A similar second network is build for the imaginary power.

Generally there are two different stages of testing; the recalling testing and the generalization testing. The recalling process includes applying the same training data as a test signal for the obtained RBFNN network.

The generalization test includes applying new data that has never been seen before by the neural network model. The

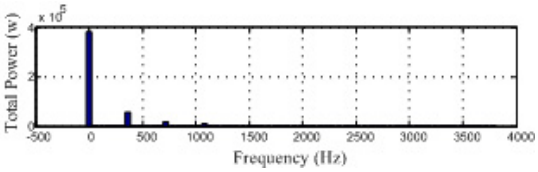

(a)

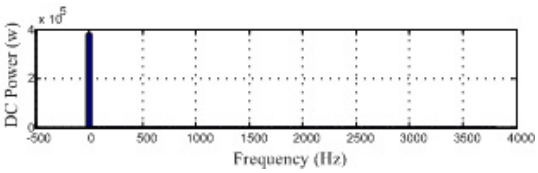

(b)

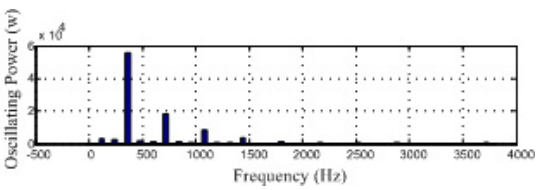

(c)

Fig. 8. FFT for the Power Signals in Fig.9. (a) Total. (b) DC Part. (c) Oscillating Part.

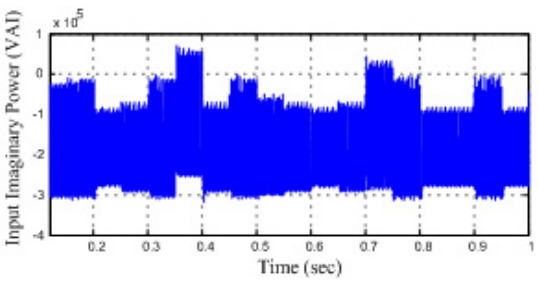

(a)

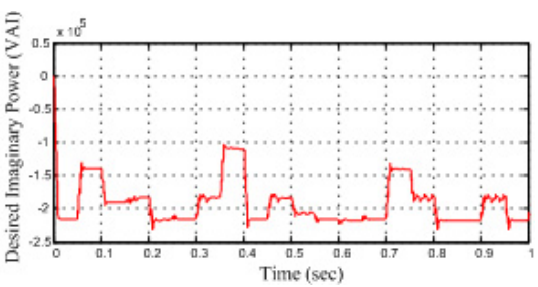

(b)

Fig. 9. Window of Training Data for the Imaginary Power RBFNN Network.

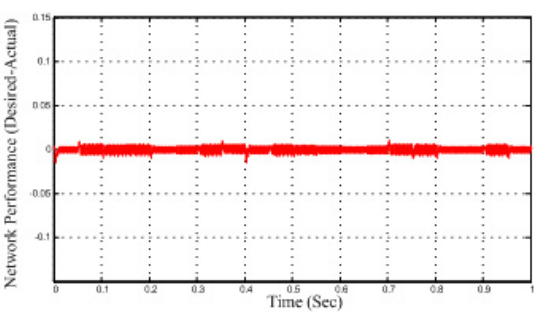

Fig. 10. q-RBFNN Network Performance for Recalling Process.

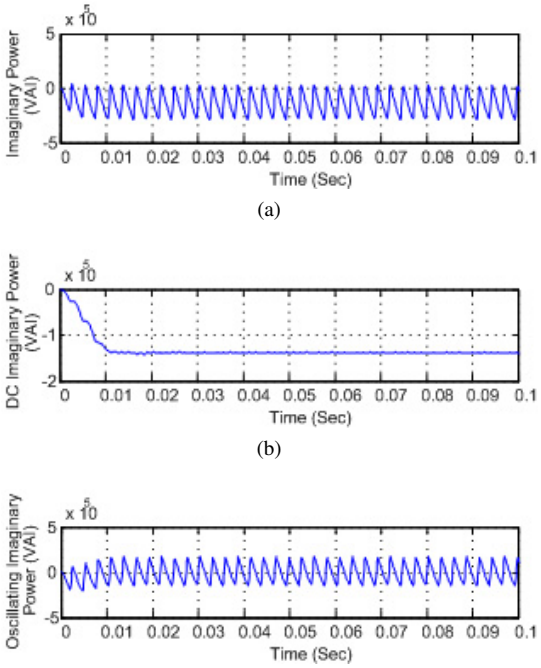

Fig. 11. Imaginary Power exchanged between the Phases. (a) Total. (b) DC Part. (c) Oscillating Part.

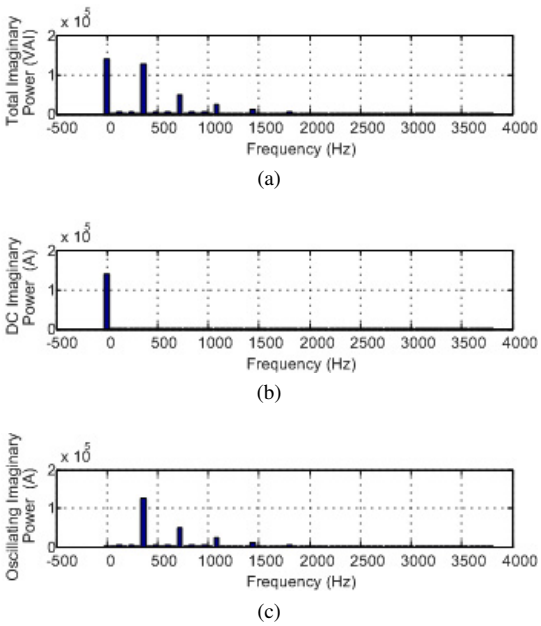

Fig. 12. FFT for the Power Signals in Fig.9. (a) (a) Total. (b) DC Part. (c) Oscillating Part.

test is performed by embedding the RBFNN model in an environment that can apply a delayed power vector as an input for the RBFNN model. Then compare the output from the RBFNN model with the actual output.

Suppose the following power signal is obtained from the system:

$$P(t) = 3VI_1\cos(\theta_1) - 3VI_5\cos(4wt - \theta_5) + 3VI_7\cos(6wt - \theta_7)$$

To make such a signal suitable for the RBFNN model, it should be sampled at the same constant rate used for the training. Then a delayed vector should be constructed in the same way as illustrated in *Appendix I.* An example of the input vector is:

$$x_k = \begin{bmatrix} p_{1k} \\ p_{2k} \\ \vdots \\ p_{Nk} \end{bmatrix}$$

Once the delayed vector is obtained, the output of the RBFNN model can be calculated based on (1) and (2) to obtain the RBFNN output y_k. Then the output $y_k$is compared with the actual output $\bar{p}(k)$ and the oscillating part can be easily found by:

$$\tilde{p}(k) = p(k) - \bar{p}(k)$$

IV. Simulation Results

The three-phase nonlinear load has the following parameters:

Voltage Source: 400 V L-L,60 Hz , source resistance 0.06 mΩ, source inductance 2 μH.

Nonlinear Load: Three-Phase thyristor rectifier with R-L load (450 kW active power, 200 kvar reactive power).

Sampling Rate: 128 sample/ cycle

RBFNN for p: 2 Hidden neurons, sigma (σ) = 71.5

RBFNN for q: 4 Hidden neurons, sigma (σ) = 42.5

The Number of inputs for p and q networks (N) = 64

The Number of Outputs for p and q networks = 1

The value of σ depends on the input training data. This value was obtained by running the simulation several times and selecting the value that minimizes the RBFNN network error.

A. Constant Active Power extraction

Fig. 5(a) shows a window from the training set for the active power obtained by the algorithm illustrated in Section III. In this training set the input for the RBFNN network is the delayed vectors of the total active power (N=64), which is calculated based on the p-q theory. Fig. 5(b) shows the desired output, which is the DC component of the delayed vector. Fig. 6 shows the performance of the network for the recalling process. The mean square error for the recalling process for the p-RBFNN is $1.49*10^{-7}$ for normalized data.

The p-RBFNN network model is tested by embedding the models inside a nonlinear SIMULINK®model. The RBFNN is used to extract the DC component of the active power, consumed by a thyristor rectifier with a R-L load. The total active power is shown in Fig. 7(a). It is clear that it has two components; a DC part, due to fundamental components, and an oscillating part, due to the harmonic content of the load current. Fig. 7(b) shows the output of the embedded RBFNN network, which is the DC part of the active power, with a minor ripple. The oscillating parts of the active power are obtained by subtracting the DC part from the total part as shown in Fig. 7(c). Fig. 8 shows the FFT analysis of the active power waveforms shown in Fig. 7. These results emphasize the robustness of the RBFNN network in decomposing the active power waveform.

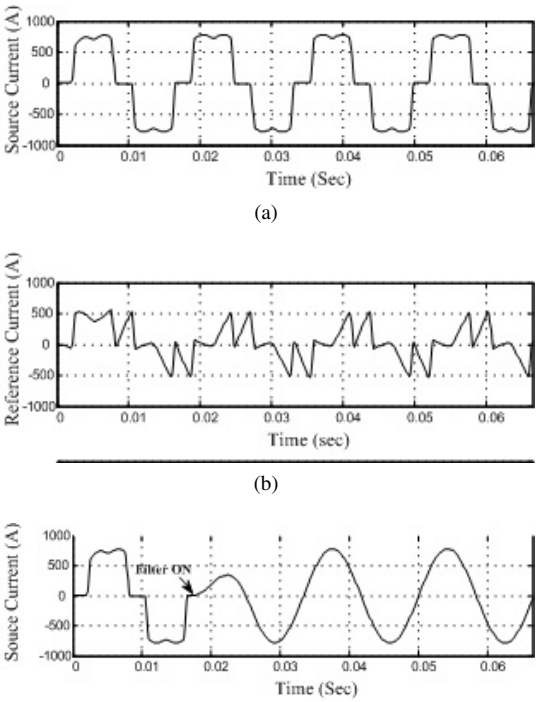

Fig. 13. phase A Source Current for Constant Power Strategy. (a) Before compensation. (b) Reference Current. (c) After Compensating.

B. Constant Imaginary Power extraction

Using a method similar to the one used for the active power, the imaginary power is decomposed into two parts; a DC part and an oscillating part using another RBFNN model. Fig. 9(a) shows a window from the training set for the imaginary power. In this training set the input for the RBFNN network is the delayed vectors of the total imaginary power (N=64). Fig. 9(b) shows the desired output, which is the DC component of the delayed vector. Fig. 10 shows the performance of the network for the recalling process. The mean square error of the recalling process for the q-RBFNN is 1.12 $*10^{-5}$ for normalized data.

The q-RBFNN is used to extract the DC component of the imaginary power, consumed by a thyristor rectifier with a R-L load. The total active power is shown in Fig. 11 (a). It is clear that it has two components; a DC part, due to the fundamental components, and an oscillating part, due to the harmonic content of the load current. Fig. 11 (b) shows the output of the embedded RBFNN network, which is the DC part of the active power, with a minor ripple. The oscillating parts, of the active power are obtained by subtracting the DC part from the total part as shown in Fig. 11(c). Fig. 12 shows the FFT analysis for the active power waveforms shown in Fig. 7. The results emphasize the robustness of the q-RBFNN network in decomposing the imaginary power waveform.

C. Constant Power Strategy

Figures 13 and 14 show the results of applying the constant power strategy where Fig.13(a) shows the phase *A* source current before compensation. Figure 13(b) shows the compensating signal (reference current). This signal is added to the source current as an output from an active power filter,

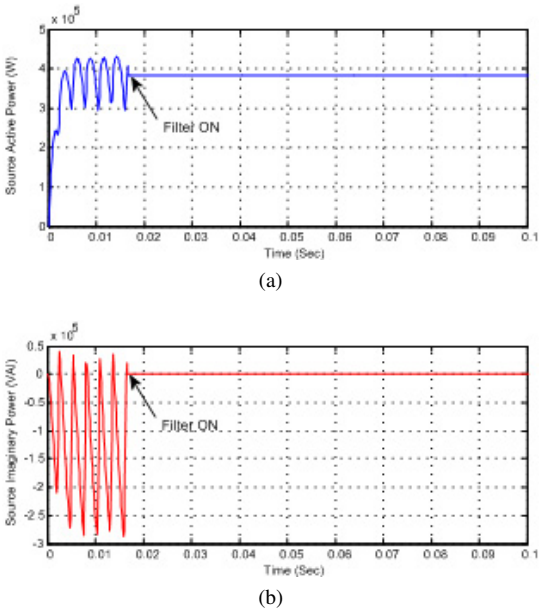

Fig. 14. Source Power for Constant Power Strategy. (a) Active Power. (b) Imaginary Power.

and the result is shown in Fig. 13(c). It is clear that the source current does not contain harmonics because it is a pure sinusoidal waveform. Fig. 14(a) shows the source active power and Fig. 14(b) shows the source imaginary power. It is clear from Fig. 11 that the source delivers only a constant active power after the filter is ON.

D. Sinusoidal Current Strategy

Fig. 15 and Fig. 16 show the results of applying the sinusoidal current strategy, where Fig. 15 (a) shows the phase *A* source current before compensation. Figure 15(b) shows the compensating signal (reference current). This signal is added to the source current as an output from an active power filter, and the result is shown in Fig. 15(c). Figure 16(a) shows the source active power and Fig. 16 (b) shows the source imaginary power.

The major difference between the two methods is that the active power filter in the first case needs to compensate for the oscillating part of the active power and the whole imaginary power, resulting in a constant source active power, with a currents that are in-phase with the supply voltages. In the second case, the active filter needs to compensate only for the oscillating parts of the active and imaginary powers, resulting in sinusoidal source currents that are not in-phase with the source voltages.

E. Disturbance Rejection

The disturbance rejection robustness of the RBFNN network is investigated with a step change in the firing angle of the Thyristor bridge, which will change the harmonics content level. Fig. 17 shows the response of the active power RBFNN network to this change. Figure 17 shows the fast response to this change (around half a cycle) and the absence of overshoot. Figure 18 shows the response of the active power RBFNN network to this change. The smooth transition reflects the robustness of the RBFNN to reject disturbances.

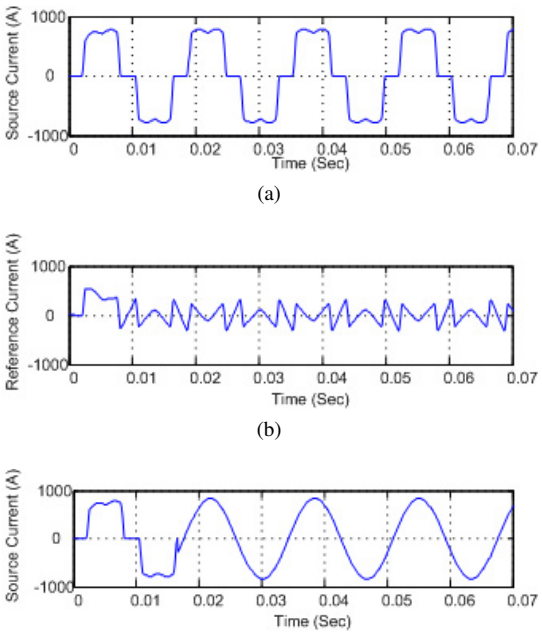

Fig. 15. phase A Source Current for Sinusoidal current Strategy. (a) Before compensation. (b) Reference Current. (C) After Compensating.

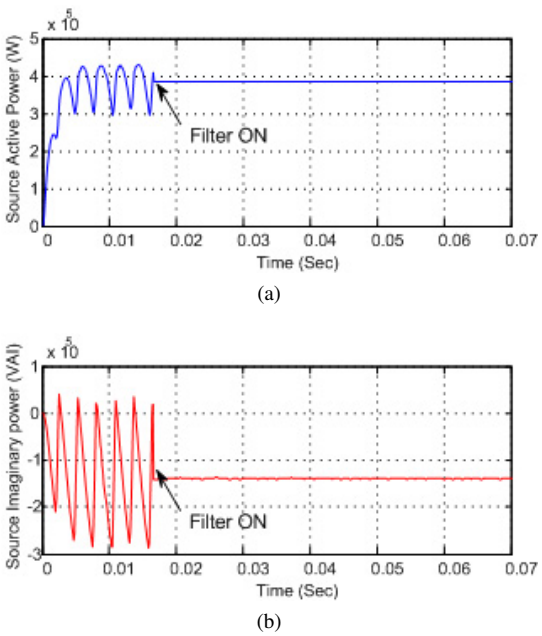

Fig. 16. Source Power for Sinusoidal Current strategy. (a) Active Power. (b) Imaginary Power.

V. Conclusions

In this paper, the RBFNN algorithm was used to extract and identify harmonics content in converter waveforms. The RBFNN training algorithm was based on the hybrid learning algorithm, which requires a short training time when compared to the conventional training methods. Two RBFNN networks were used to decompose the active power and the imaginary power into their DC and oscillating components. The algorithms were based on the p-q power theory, which gives flexibility in the choosing of a compensation strategy. The constant power and sinusoidal current compensation strategies were investigated. The results show good performance for

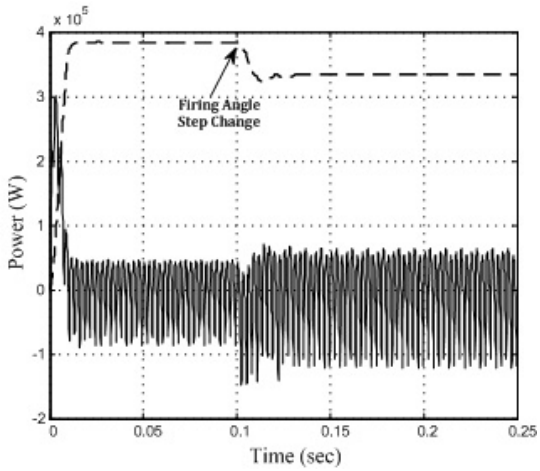

Fig. 17. p- RBFNN Network Response for a Firing Angle Step Change from 10^o -20^o. DC Power (Dashed), Oscillating Power (Solid).

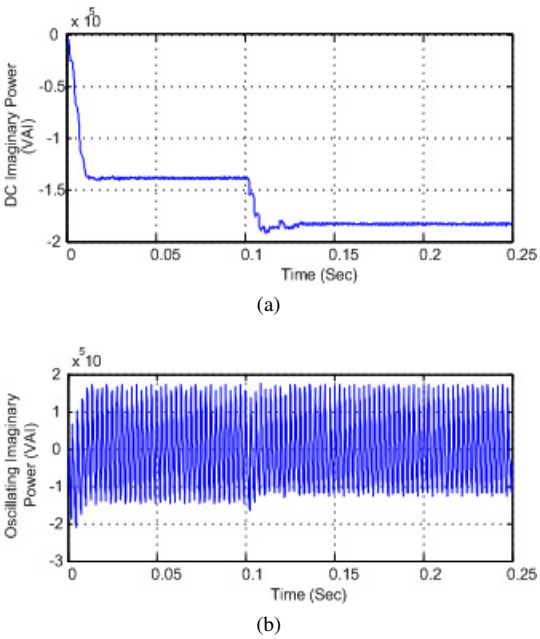

Fig. 18. q-RBFNN Network Response for a Firing Angle Step Change from 10^o -20^o.(a) DC Imaginary Power. (b) Oscillating Imaginary Power.

decomposing the active and imaginary power. The algorithms performed very well in both transient and steady-state conditions. The simulations also showed that the methodology outlined here can be used to dynamically identify harmonics and for the elimination of harmonics using active power filters.

APPENDIX I

p-q Theory

Consider the three-phase controlled rectifier with an R-L load shown in Fig. 3. A uniformly distributed random gating signal is applied to the three-phase rectifier. The voltages and currents of the rectifier are sampled and used to calculate the instantaneous active power p and imaginary power q based on the p-q theory. The Clark transformation is used to transform the voltages and currents from the a-b-c domain to the α-β

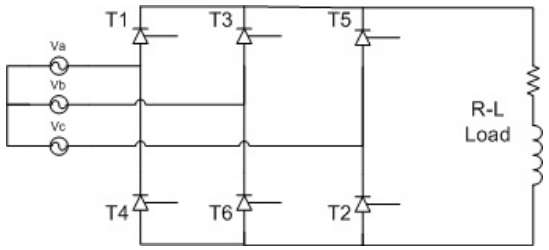

Fig. 19. Schematic Diagram for Three-Phase controlled Converter.

domain, as shown in (13) and (14).

$$\begin{bmatrix} v_\alpha \\ v_\beta \end{bmatrix} = \sqrt{\frac{2}{3}} \begin{bmatrix} 1 & -1/2 & -1/2 \\ 0 & \sqrt{3}/2 & -\sqrt{3}/2 \end{bmatrix} \begin{bmatrix} v_a \\ v_a \\ v_a \end{bmatrix} \quad (13)$$

$$\begin{bmatrix} i_\alpha \\ i_\beta \end{bmatrix} = \sqrt{\frac{2}{3}} \begin{bmatrix} 1 & -1/2 & -1/2 \\ 0 & \sqrt{3}/2 & -\sqrt{3}/2 \end{bmatrix} \begin{bmatrix} i_a \\ i_a \\ i_a \end{bmatrix}. \quad (14)$$

Then p and q are calculated from the α-β domain voltages and the current as shown in (15).

$$\begin{bmatrix} p \\ q \end{bmatrix} = \begin{bmatrix} v_\alpha & v_\beta \\ -v_\beta & v_\alpha \end{bmatrix} \begin{bmatrix} i_\alpha \\ i_\beta \end{bmatrix}. \quad (15)$$

The instantaneous p and q can be decomposed into the following:

$$p = \tilde{p} + \bar{p} \quad (16)$$

$$q = \tilde{q} + \bar{q} \quad (17)$$

here $\bar{p}$ is the constant part of p (which comes from the fundamental components), $\tilde{p}$ is the oscillating part of p (which comes from the harmonics), and in similar fashion $\bar{q}$ and $\tilde{q}$ are the constant and oscillating parts of q.

In this paper two compensation strategies have been applied [13]. The first is called the *constant power* strategy. In this strategy the oscillating part of the active power $\tilde{p}$ is extracted. The resulting reference power signal contains $\tilde{p}$ plus power losses (p_{loss}) (always present), and the total imaginary power q is shown as p_{ref} and q_{ref} in (18) and (19), respectively.

$$p_{ref} = \tilde{p} + p_{loss} \quad (18)$$

$$q_{ref} = q = \tilde{q} + \bar{q}. \quad (19)$$

The second compensation strategy, used in this paper, is called the *sinusoidal current* strategy. Here both of the oscillating parts $\tilde{p}$ and $\tilde{q}$ are extracted. The resulting reference power signal contains $\tilde{p}$ plus p_{loss} (additional power losses are present) and $\tilde{q}$ is shown as p_{ref} and q_{ref} in (20) and (21), respectively.

$$p_{ref} = \tilde{p} + p_{loss} \quad (20)$$

$$q_{ref} = \tilde{q}. \quad (21)$$

The reference current in the α-β domain can be calculated by:

$$\begin{bmatrix} i_{\alpha ref} \\ i_{\beta ref} \end{bmatrix} = \begin{bmatrix} v_\alpha & v_\beta \\ -v_\beta & v_\alpha \end{bmatrix}^{-1} \begin{bmatrix} i_\alpha \\ i_\beta \end{bmatrix} \quad (22)$$

$$\begin{bmatrix} i_{aref} \\ i_{bref} \\ i_{cref} \end{bmatrix} = \sqrt{\frac{2}{3}} \begin{bmatrix} 1 & 0 \\ -1/2 & \sqrt{3}/2 \\ -1/2 & -\sqrt{3}/2 \end{bmatrix} \begin{bmatrix} i_{\alpha ref} \\ i_{\beta ref} \end{bmatrix}. \quad (23)$$

Example

Consider a three-phase system with a sinusoidal balanced voltage and a balanced nonlinear load as follows:

$$V_a(t) = \sqrt{2}Vsin(wt), V_b(t) = \sqrt{2}Vsin(wt - \frac{2\pi}{3}),$$

$$V_c(t) = \sqrt{2}Vsin(wt + \frac{2\pi}{3})$$

$$I_a(t) = \sqrt{2}I_1 sin(wt - \theta_1) - \sqrt{2}I_5 sin(5wt - \theta_5) + \sqrt{2}I_7 sin(7wt - \theta_7)$$

$$I_b(t) = \sqrt{2}I_1 sin(wt - \frac{2\pi}{3} - \theta_1) - \sqrt{2}I_5 sin(5wt + \frac{2\pi}{3} - \theta_5) + \sqrt{2}I_7 sin(7wt - \frac{2\pi}{3} - \theta_7)$$

$$i_c(t) = \sqrt{2}I_1 sin(wt + \frac{2\pi}{3} - \theta_1) - \sqrt{2}I_5 sin(5wt - \frac{2\pi}{3} - \theta_5) + \sqrt{2}I_7 sin(7wt + \frac{2\pi}{3} - \theta_7)$$

Using (13) and (14) the voltage and current in the α-β domain can be calculated as:

$$V_\alpha(t) = \sqrt{3}Vsin(wt), V_\beta(t) = -\sqrt{3}Vcos(wt)$$

$$i_\alpha(t) = \sqrt{3}I_1 sin(wt - \theta_1) - \sqrt{3}I_5 sin(5wt - \theta_5) + \sqrt{3}I_7 sin(7wt - \theta_7)$$

$$i_\alpha(t) = \sqrt{3}I_1 cos(wt - \theta_1) - \sqrt{3}I_5 cos(5wt - \theta_5) + \sqrt{3}I_7 cos(7wt - \theta_7)$$

The instantaneous p and q are calculated from (15) as:

$$P(t) = 3VI_1 cos(\theta_1) - 3VI_5 cos(4wt - \theta_5) + 3VI_7 cos(6wt - \theta_7)$$

$$q(t) = 3VI_1 sin(\theta_1) - 3VI_5 sin(4wt - \theta_5) + 3VI_7 sin(6wt - \theta_7)$$

It is clear that both p and q have two parts; constant parts ($\bar{p}$ and $\bar{q}$) and oscillating parts ($\tilde{p}$ and $\tilde{q}$), where:

$$\bar{p} = 3VI_1 cos(\theta_1), \bar{q} = 3VI_1 sin(\theta_1)$$

$$\tilde{p} = -3VI_5 cos(4wt - \theta_5) + 3VI_7 cos(6wt - \theta_7)$$

$$\tilde{q} = -3VI_5 sin(4wt - \theta_5) + 3VI_7 sin(6wt - \theta_7)$$

The reference values are then computed from (22) and (23).

REFERENCES

[1] M. Izhar, C. M. Hadzer, S. Masri and S. Idris, "A study of the fundamental principles to power system harmonic," in Power Engineering Conference, 2003. PECon 2003. Proceedings. National, pp. 225-232, 2003.

[2] J. S. Subjak Jr. and J. S. McQuilkin, "Harmonics-causes, effects, measurements, and analysis: an update," IEEE Trans. Ind. Appl., Vol. 26, pp. 1034-1042, Nov./Dec. 1990.

[3] Sumaryadi, H. Gumilang and, and A. Suslilo, "Effect of power system harmonic on degradation process of transformer insulation system," in Properties and Applications of Dielectric Materials, ICPADM 2009. IEEE 9th International Conference on the, pp. 261-264, 2009.

[4] S. Rahmani, A. Hamadi, and K. Al-Haddad, "A new combination of shunt hybrid power filter and thyristor controlled reactor for harmonics and reactive power compensation," in Electrical Power & Energy Conference (EPEC), pp. 1-6, 2009.

[5] H. Akagi, "New trends in active filters for power conditioning," IEEE Trans. Ind. Appl., Vol. 32, pp. 1312-1322, Nov./Dec. 1996.

[6] M. El-Habrouk, M. K. Darwish, and P. Mehta, "Active power filters: a review," Electric Power Applications, IEE Proceedings , Vol. 147, pp. 403-413, 2000.

[7] T. C. Green and J. H. Marks, "Control techniques for active power filters," Electric Power Applications, IEE Proceedings, Vol. 152, pp. 369-381, 2005.

[8] B. Singh, K. Al-Haddad, and A. Chandra, "A review of active filters for power quality improvement," IEEE Trans. Ind. Electron., Vol. 46, pp. 960-971, Oct. 1999.

[9] G. W. Chang, C.-I. Chen and Y.-F. Teng, "Radial-Basis-Function-Based Neural Network for Harmonic Detection," IEEE Trans. Ind. Electron., Vol. 57, pp. 2171-2179, Jun. 2010.

[10] A. Zouidi, F. Fnaiech, K. Al-Haddad and S. Rahmani, "Adaptive linear combiners a robust neural network technique for on-line harmonic tracking," in Industrial Electronics, 2008. IECON, pp. 530-534, 2008.

[11] S. S. Haykin, 1931- Neural Networks : A Comprehensive Foundation, Upper Saddle River, N.J. : Prentice Hall, 1999.

[12] N. K. Kasabov, Foundations of Neural Networks, Fuzzy Systems, and Knowledge Engineering , Cambridge, Mass. : MIT Press, 1996.

[13] H. Akagi, Instantaneous Power Theory and Applications to Power Conditioning, Hoboken: John Wiley Sons, 2007.

[14] J. Moody, "Fast learning in networks of locally-tuned processing units," Neural Comput., Vol. 1, pp. 281, 1989.

[15] R. Yousef, "Training radial basis function networks using reduced sets as center points," International Journal of Information Technology, Vol. 2, pp. 21, 2005.

Eyad K. Almaita (SM'2010) received his B.S. from the Al-Balqa Applied University, Jordan, in 2000, and his M.S. from Al-Yarmouk University, Jordan, in 2006. He is now perusing his Ph.D. in Electrical and Computer Engineering at Western Michigan University. His current research interests include power electronics, control engineering, artificial intelligence and microprocessor / microcontroller embedded applications.

Johnson A. Asumadu (S'82, M'94, SM'00) received his B.S. from the University of Science Technology, Ghana, in 1975, his M.S. from Aston University, England, in 1978, his MEE from the Rensselaer Polytechnic Institute, USA, in 1983, and his Ph.D. from the University of Missouri-Columbia, USA, in 1987. He is now a faculty member at Western Michigan University, Michigan. He has published several technical papers and books, has a number of patents and has been involved in numerous government and industrial-sponsored projects. His current research interests include power electronics and control engineering including fuzzy logic applications, and microprocessor / microcontroller embedded applications.